Correlation of Subcellular Compartmentalization of HPMA Copolymer-Mce$_6$ Conjugates with Chemotherapeutic Activity in Human Ovarian Carcinoma Cells

Monica Tijerina,[1] Pavla Kopečková,[1,2] and Jindřich Kopeček[1,2,3]

Received October 17, 2002; accepted February 3, 2003

Purpose. Intracellular targets sensitive to oxidized damage generated by photodynamic therapy (PDT) utilizing N-(2-hydroxypropyl)methacrylamide (HPMA) copolymer-mesochlorin e_6 monoethylenediamine (Mce$_6$) conjugates was explored to aid in the design of second-generation PDT delivery systems.

Methods. Low temperature, metabolic inhibitor, and nuclear localization sequences (NLS(FITC)) were used to achieve desired subcellular localization that was evaluated by confocal analysis and subcellular fractionation. Mce$_6$ was bound to HPMA copolymer conjugates via non-degradable dipeptide linkers (P-GG-Mce$_6$, P-NLS(FITC)-GG-Mce$_6$) or lysosomally degradable tetrapeptide spacers (P-GFLG-Mce$_6$, P-NLS(FITC)-GFLG-Mce$_6$). Chemotherapeutic efficacy was assessed by the concentration that inhibited growth by 50% (IC_{50}), cell associated drug concentration (CAD) and confocal microscopy.

Results. P-GFLG-Mce$_6$ possessed enhanced chemotherapeutic activity compared to P-GG-Mce$_6$ indicating enzymatically released Mce$_6$ was more active than copolymer-bound Mce$_6$. Lysosomes appeared less sensitive to photodamage as observed by a higher IC_{50}. Nuclear-directed HPMA copolymer-Mce$_6$ conjugates (P-NLS(FITC)-GG-Mce$_6$, P-NLS(FITC)-GFLG-Mce$_6$) possessed enhanced chemotherapeutic activity. However, control cationic HPMA copolymer-Mce$_6$ conjugates containing a scrambled NLS (P-scNLS(FITC)-GG-Mce$_6$) or amino groups (P-NH$_2$-GG-Mce$_6$) also displayed increased chemotherapeutic activity.

Conclusions. Nuclear delivery was observed for P-NLS(FITC)-GG-Mce$_6$ and P-NLS(FITC)-GFLG-Mce$_6$ indicating NLS was a feasible approach for nuclear delivery. Due to the cationic nature of NLS, increased membrane binding of PDT systems incorporating cationic nuclear targeting moieties must be addressed.

KEY WORDS: N-(2-hydroxypropyl)methacrylamide (HPMA); photodynamic therapy (PDT); mesochlorin e_6 monoethylenediamine (Mce$_6$); nuclear localization sequences (NLS).

INTRODUCTION

PDT is an emerging mode of therapy involving the excitation of photosensitizers by a specific wavelength of light at the site of neoplastic growth. On excitation, triplet state photosensitizers liberate energy by way of proton abstraction or donation with surrounding substrate generating radicals (Type I) or by energy transfer with molecular oxygen producing singlet oxygen, a reactive form of molecular oxygen (Type II). Both pathways elicit damage at the site of photoactivation; however, singlet oxygen has been shown to be the predominant species on photoactivation of porphyrins. Because of the short half-life of singlet oxygen (~4 μsec), photodamage is limited to within approximately 0.1 μm of the site of photoactivation (1). To design optimum PDT delivery systems, it is essential to initially accumulate photosensitizers into tumor tissue and subsequently target PDT sensitive subcellular targets within neoplastic cells to diminish side-effects associated with non-specific damage to normal tissue (2).

Photosensitizers have shown specificity for tumor uptake (3), but delivery of sensitizers by way of a macromolecular delivery system can dramatically enhance tumor accumulation because of enhanced permeability and retention of macromolecules within tumors (4). Morphologic examination of tumor vessels in humans have shown discontinuous or absent basement membrane, excessive spatial heterogeneity, and wide interendothelial junctions resulting in enhanced permeability (5). Additionally, solid tumors possess an impaired lymphatic drainage system resulting in accumulation of macromolecules. Although outward convective flow of HPMA copolymer-Mce$_6$ conjugates is possible because of elevated interstitial fluid pressure within tumors (6), biodistribution studies have shown preferential accumulation of conjugates within tumor xenografts in mice (7). HPMA copolymers are attractive macromolecular delivery systems as they are biocompatible, extend the margin of safety of free Mce$_6$, overcome multidrug resistance, passively accumulate in tumors, and can be easily synthesized to actively target tumor cells and PDT sensitive subcellular organelles within cancer cells (8).

Targeting HPMA copolymer-Mce$_6$ conjugates utilizing antibody or antibody Fab′ fragments toward human ovarian OVCAR-3 cells enhanced tumor uptake dramatically reduc-

[1] Departments of Pharmaceutics and Pharmaceutical Chemistry/CCCD, University of Utah, 30S 2000E Room 301, Salt Lake City, Utah 84112.

[2] Department of Bioengineering, University of Utah, Salt Lake City, Utah 84112.

[3] To whom correspondence should be addressed. (e-mail: Jindrich.Kopecek@m.cc.utah.edu)

ABBREVIATIONS: AIBN, 2,2′-azobisisobutyronitrile; CAD, cell associated drug concentration; DMF, N,N-dimethylformamide; DNP, 2,4-dinitrophenol; FITC, fluorescein-5-isothiocyanate; GFLG, glycylphenylalanylleucylglycine; GG, glycylglycine; HPMA, N-(2-hydroxypropyl)methacrylamide; IC_{50}, concentration that inhibits growth 50%; MA, methacryloyl; MAL, maleimido groups; Mce$_6$, mesochlorin e_6 monoethylenediamine; MeOH, methanol; NLS, nuclear localization sequences; ONp, *p*-nitrophenoxy; P, HPMA copolymer backbone; PDT, photodynamic therapy; P-GFLG-Mce$_6$, HPMA copolymer-Mce$_6$ conjugates containing Mce$_6$ bound by way of GFLG linker; P-GG-Mce$_6$, HPMA copolymer-Mce$_6$ conjugates containing Mce$_6$ bound by way of GG linker; PI, propidium iodide; P-NLS(FITC), HPMA copolymer containing NLS(FITC) bound by way of a thioether linkage; P-NLS(FITC)-GFLG-Mce$_6$, HPMA copolymer-Mce$_6$ conjugates containing Mce$_6$ bound by way of a GFLG spacer and containing NLS(FITC) bound by way of a thioether linkage P-NLS(FITC)-GG-Mce$_6$, HPMA copolymer-Mce$_6$ conjugates containing Mce$_6$ bound by way of a GG spacer and containing NLS(FITC) bound by way of a thioether linkage; P-Texas Red, HPMA copolymer containing bound Texas Red; SMCC, succinimidyl *trans*-4-(maleimidylmethyl)cyclohexane- 1-carboxylate; SAMSA, 5-((2-(and-3)-*S*-(acetylmercapto)succinoyl) amino)fluorescein assay; WST-8, 2-(2-methoxy-4-nitrophenyl)-3-(4-nitrophenyl)-5-(2,4-disulfophenyl)-2H-tetrazolium monosodium salt.

0724-8741/03/0500-0728/0 © 2003 Plenum Publishing Corporation

ing the IC_{50} up to 700-fold compared to non-targeted HPMA copolymer-Mce$_6$ conjugates (9). Subsequently, targeting HPMA copolymer-Mce$_6$ conjugates to PDT sensitive subcellular organelles may further enhance chemotherapeutic activity. Nuclear-targeted chlorin e_6 delivery systems utilizing constructs containing nuclear localization sequences (NLS) from simian virus large tumor antigen has been shown to dramatically improve anticancer activity up to 2000-fold *in vitro* (10,11).

Here we examined the sensitivity of various subcellular targets in human ovarian carcinoma A2780 cells to PDT. HPMA copolymer-Mce$_6$ conjugates were designed and synthesized to elucidate PDT sensitive organelles. Mce$_6$ was bound to HPMA copolymer-Mce$_6$ conjugates utilizing a non-degradable dipeptide linker (GG) or a lysosomally degradable tetrapeptide spacer (GFLG). Due to the large molecular weight of HPMA copolymer-Mce$_6$ conjugates (~20 kDa), cellular uptake was limited to pinocytosis that resulted in accumulation within endocytic vesicles. Lysosomal accumulation of P-GFLG-Mce$_6$ resulted in the enzymatic release of free Mce$_6$ primarily by cathepsin B (12). To distinguish sensitivity between lysosomes and plasma membrane to PDT, low temperature and metabolic inhibitors (2,4-dinitrophenol, DNP) were used to prevent endocytic uptake of P-GG-Mce$_6$ (13). Nuclei were targeted by way of the covalent attachment of a minimal NLS (PKKKRKV$_{132}$K(FITC)C) from simian virus large tumor antigen to HPMA copolymer-Mce$_6$ conjugates. Preferential subcellular accumulation of HPMA copolymer-Mce$_6$ conjugates was confirmed qualitatively by confocal microscopy and semi-quantitatively by way of subcellular fractionation. Chemotherapeutic activity of HPMA copolymer-Mce$_6$ conjugates localized in preference to different subcellular compartments and assessed in A2780 human ovarian carcinoma cells, whereas morphologic evaluation of subcellular organelles following PDT was evaluated by confocal microscopy. These studies help to correlate photoactivation of HPMA copolymer-Mce$_6$ conjugates preferentially accumulated to various intracellular targets with chemotherapeutic efficacy.

MATERIALS AND METHODS

Cell Lines

Human ovarian A2780 cells were obtained from T. C. Hamilton (Fox Chase Cancer Center, PA, USA). Cells were cultured in RPMI 1640 medium (Sigma) supplemented with 10% fetal bovine serum (FBS, Hyclone) and 10 μg/mL insulin (Sigma) at 37°C in a humidified atmosphere of 5% CO_2 (v/v).

Monomers

MA-GG-Mce$_6$, a polymerizable derivative of Mce$_6$, was obtained by aminolysis of N-methacryloyldiglycyl p-nitrophenyl ester with Mce$_6$ disodium salt. Thirty-five mg (0.11 mmol) of MA-GG-ONp was dissolved in 0.8 ml of DMF, then 68 mg (0.10 mmol) of Mce$_6$ was added as a solid, followed by the addition of 20 μl diisopropylethylamine. The reaction mixture was stirred for 24 h, the solvent was removed *in vacuo* and the solid was triturated several times with ether. The yield was 68 mg. TLC, R_f:0.52 ($CHCl_3$:MeOH:AcOH, 3:1:0.1), and ES-MS (m/z: M^+ 823.3) confirmed the structure.

MA-GFLG-Mce$_6$ was synthesized as previously described (9).

Polymer Precursors

HPMA copolymer containing amino groups (P-NH_2) was prepared by copolymerization of HPMA (14) with N-(3-aminopropyl)methacrylamide hydrochloride using 2,2′-azobisisobutyronitrile (AIBN) as the initiator and 3-mercaptopropionic acid as the chain transfer agent (molar ratio: 94:6:4:0.4, respectively) in MeOH (10 wt.% monomers in the mixture) at 50°C for 24 h. The polymer was isolated by precipitation into ether, then extensively dialyzed (M_W cut off 6–8 kDa) and freeze-dried. The polymer contained 5.3 mol % (0.35 mmol/g) of amino groups containing side-chains as determined by a Ninhydrin method using the amino containing monomer as a calibration sample.

Polymer precursors containing side-chains terminated in reactive p-nitrophenyl ester groups were prepared by radical precipitation copolymerization of HPMA with N-methacroylglycylglycine p-nitrophenyl ester (P-GG-ONp) or N-methacroylglycylphenylalanylleucylglycine p-nitrophenyl ester (P-GFLG-ONp) (15) in acetone in the presence of AIBN (16).

HPMA Copolymer Conjugates

The structure and composition of HPMA copolymer conjugates are summarized in Fig. 1 and Table I. Their synthesis is described below.

P-Texas Red (P1). Texas Red labeled HPMA copolymer conjugate was prepared by reacting P-NH_2 (115 mg, 0.040 mmol NH_2 groups, in 0.8 ml DMF) with 10 mg (0.012 mmol) of Texas Red succinimidyl ester (mixed isomers Molecular Probes T-6134) followed by the addition of 8.4 mg (0.083 mmol) of triethylamine. The reaction was stirred for 3 h at room temperature. Residual amino groups were reacted with an excess of succinic anhydride (50 mg), followed by the addition of 20 mg triethylamine. The polymer was purified first on a Sephadex LH-20 column in MeOH, then by extensive dialysis (M_W cut off 12–14 kDa). The freeze-dried product contained 1.5 mol % Texas Red containing side-chains (0.090

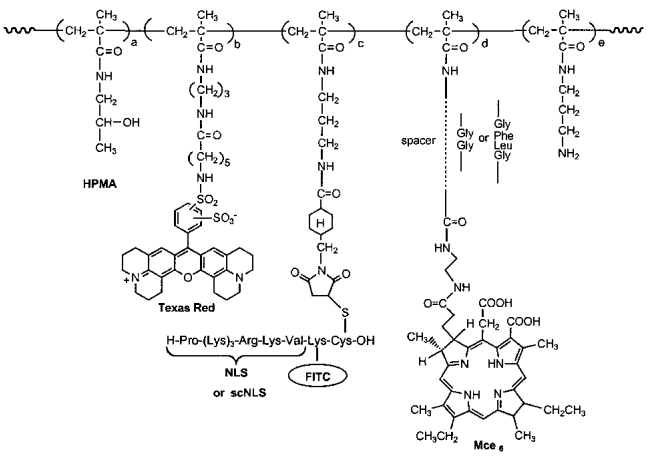

Fig. 1. Structure and composition of HPMA copolymer conjugates.

Table I. Composition of HPMA Copolymer Conjugates

	Conjugates	a	b	c	d	e	M.W. (kDa)
P1	P-Texas Red	98.4	1.6				26
P2	P-NLS(FITC)	98.5		1.5			26
P3	P-GG-Mce_6	97.0			3.0		21
P4	P-NLS(FITC)-GG-Mce_6	96.5		1.2	2.3		26
P5	P-scNLS(FITC)-GG-Mce_6	96.2		1.4	2.4		26
P6	P-NH_2-GG-Mce_6	92.9			2.2	4.9	26
P7	P-GFLG-Mce_6	98.5			1.5		22
P8	P-NLS(FITC)-GFLG-Mce_6	97.2		1.4	1.4		26

Note: Synthesis of HPMA copolymer-Mce_6 conjugates is described in Materials and Methods.

mmol Texas Red/g; determined spectrophotometrically, ε = 116000 M^{-1} cm^{-1}, 585 nm, MeOH).

P-NLS(FITC) (P2). HPMA copolymer-NLS conjugate was prepared in two steps. First, an HPMA copolymer containing maleimide groups (P-MAL) was obtained by reaction of 100 mg of P-NH_2 (0.035 mmol NH_2 groups) with 23.4 mg (0.070 mmol) of succinimidyl *trans*-4-(maleimidylmethyl)cyclohexane-1-carboxylate (SMCC) and 11 mg (0.09 mmol) of diisopropylethylamine in DMF at room temperature by stirring for 12 h. The solvent was removed *in vacuo* and polymer was precipitated into acetone. The content of maleimide groups, 0.29 mmol/g, was determined by a 5-((2-(and-3)-*S*-(acetylmercapto)succinoyl) amino)fluorescein assay (SAMSA assay, Molecular Probes). In the second step, P-NLS(FITC) (P2) was obtained by reaction of 41 mg of P-MAL (0.012 mmol MAL groups) in 0.8 ml of phosphate buffered saline (PBS) pH 7.0 with 9.3 mg (0.006 mmol) of NLS dissolved in 0.2 ml of PBS. The reaction mixture was stirred overnight at room temperature, then 5 μl of mercaptoethanol was added to inactivate the residual maleimide groups and polymer was separated on a Sephadex G-25 (PD-10 column) in PBS. The polymer was dialyzed (M_W cut off 12–14 kDa) first against 1 mM HCl then DI water and isolated by freeze-drying (yield 42 mg). The content of bound NLS (0.060 mmol/g) was determined by spectrophotometric determination of FITC using ε = 80000 $M^{-1}cm^{-1}$ in 0.1 M sodium borate.

P-GG-Mce_6 (P3). HPMA copolymer containing Mce_6 bound via a non-degradable glycylglycine spacer (P-GG-Mce_6, P3) was synthesized by aminolysis of polymeric precursor P-GG-ONp with free Mce_6 (Porphyrin Products) in anhydrous DMSO. Unreacted ONp was removed by way of the addition of 1-amino-2-propanol. P3 was precipitated into acetone, purified on a LH-20 column and lyophilized. Mce_6 content was evaluated by spectrophotometric determination of Mce_6 utilizing ε = 158000 $M^{-1}cm^{-1}$ at 395 nm in MeOH.

P-NLS(FITC)-GG-Mce_6 (P4). HPMA copolymer-Mce_6 conjugate containing Mce_6 bound by a glycylglycine spacer and containing NLS(FITC) bound utilizing a thioether bond was prepared in two steps. First, an HPMA copolymer-Mce_6 conjugate containing amino groups was prepared by copolymerization of HPMA, MA-GG-Mce_6, and N-(3-aminopropyl)methacrylamide hydrochloride. Next, the NLS-(FITC) sequences were attached similarly as described for P2. Conjugate P4 contained 0.127 mmol Mce_6/g (GG) and 0.065 mmol NLS/g.

P-scNLS(FITC)-GG-Mce_6 (P5). HPMA copolymer-Mce_6 conjugate containing Mce_6 bound via a glycylglycine spacer and containing scNLS(FITC) bound via a thioether bond was prepared as described for P4 with the replacement of the NLS with a scNLS ($KPRKVKK_{132}K$(FITC)C, Emory University, USA). Conjugate P5 contained 0.130 mmol Mce_6/g (GG) and 0.074 mmol scNLS/g.

P–NH_2-GG-Mce_6 (P6). HPMA copolymer containing randomly distributed amino groups and Mce_6 bound through a non-degradable GG spacer was prepared by copolymerization of HPMA with MA-GG-Mce_6 and N-(3-aminopropyl)methacrylamide hydrochloride in the molar ratio 92:3:5 using the same procedure as described above (without addition of the chain transfer agent). The polymer contained 0.33 mmol NH_2/g polymer and 0.11 mmol Mce_6/g polymer. This polymer was used as a precursor for the synthesis of P4 and P5.

P-GFLG-Mce_6 (P7). HPMA copolymer containing Mce_6 bound by a degradable glycylphenylalanylleucylglycine spacer (P-GFLG-Mce_6, P7) was synthesized by aminolysis of polymeric precursor P-GFLG-ONp with free Mce_6 (Porphyrin Products) in anhydrous DMSO similarly as described for P3.

P-NLS(FITC)-GFLG-Mce_6 (P8). HPMA copolymer-Mce_6 conjugate containing Mce_6 bound by way of a GFLG spacer and containing NLS(FITC) bound by way of a thioether bond was prepared in two steps. First, an HPMA copolymer-Mce_6 conjugate containing amino groups was prepared by copolymerization of HPMA, MA-GFLG-Mce_6, and N-(3-aminopropyl)methacrylamide hydrochloride. Next, the NLS(FITC) sequences were attached similarly as described for P2. Conjugate P8 contained 0.1 mmol Mce_6/g (GFLG) and 0.072 mmol NLS/g.

The molecular weight of polymers was determined by size exclusion chromatography using ÄKTA system, equipped with a Superose 6 HR 10/30 column calibrated with polyHPMA samples, in buffer 30% CH_3CN in PBS. The M_w of polymers were between 25–50 kDa and the polydispersity (M_w/M_n) ranged from 1.4–1.6.

Confocal Microscopy

Internalization and compartmentalization of fluorescently labeled HPMA copolymer conjugates and subcellular damage induced on illumination were monitored utilizing a Zeiss (Thornwood, NY, USA) LSM 510 confocal imaging system.

For internalization and compartmentalization, P-Texas Red (P1) and P-NLS(FITC) (P2) served as model HPMA copolymer conjugates. Both Texas Red and NLS(FITC) were bound via non-degradable spacers to monitor the fate of HPMA copolymer carriers. Three hundred thousand A2780 cells were sub-cultured into 6 well plates containing sterile cover slips and incubated overnight in a humidified atmosphere containing 5% CO_2. P-Texas Red (P1, 100 μg/mL) or P-NLS(FITC) (P2, 100 μg/mL) was exposed to cells at either 4°C, 37°C or at 37°C in the presence of DNP (50 μg/mL). Cells were washed several times with ice-cold PBS and fixed with 4% paraformaldehyde for 20 min at 37°C. For counterstaining with propidium iodide (PI, Molecular Probes), cells were treated with 0.1% Triton for 4 min, treated with DNase-free RNase (100 μg/mL, Sigma) for 20 min at 37°C and incubated with PI (100 μg/mL) for 20 min at room temperature.

Cover slips were inverted onto microscope slides utilizing anti-fade reagent (Molecular Probes) and kept at 4°C until analysis.

To evaluate subcellular damage induced on illumination, three hundred thousand A2780 cells were sub-cultured into 6 well plates containing sterile cover slips and incubated overnight in a humidified atmosphere containing 5% CO_2. The IC_{50} of free Mce_6 or HPMA copolymer-Mce_6 conjugates was incubated with cells for 4 h, media containing drug or drug conjugate was removed and cells were immediately illuminated for 30 min (3 mW/cm^2) and incubated in a humidified atmosphere containing 5% CO_2 for 4 h. Half an hour before fixation procedure, nuclei, mitochondria, and lysosomes were labeled with Hoechst 33342 (1 μM, Molecular Probes), MitoFluor™ Far Red (1 μM, Molecular Probes), and LysoTracker® Green DND-26 (2 μM, Molecular Probes), respectively. Cells were rinsed several times with ice-cold PBS, fixated with 4% paraformaldehyde for 20 min at 37°C and rinsed several times with PBS. The cover slips were inverted onto microscope slides utilizing anti-fade reagent (Molecular Probes) and stored at 4°C until analysis. Untreated control cells were incubated with Hoechst 33342, MitoFluor™ Far Red and LysoTracker® Green DND-26 as described to confirm distinct fluorescence of organelle probes.

Subcellular Fractionation

Percoll was used as the density gradient medium to separate subcellular organelles. Ten million cells were subcultured into 75cm^2 tissue culture treated flasks. The following day, cells were exposed to HPMA copolymer-Mce_6 conjugates (100 μM of Mce_6 equivalent) for 4 h, rinsed several times with ice-cold PBS, scrapped and centrifuged at 800× g for 10 min. Cells were re-suspended in 0.25 M sucrose, 10 mM Tris-HCl, 1 mM EDTA, pH 7.2 and homogenized with a ball-bearing homogenizer. The homogenate was centrifuged at 800× g for 10 min and the supernatant was applied to 23% Percoll, centrifuged at 59,000× g for 25 min and fractionated with a peristaltic pump into 8 fractions (~1.2 mL). The pellet from the homogenization process was further purified by resuspending in 0.25 M sucrose, 10 mM Tris-HCl, 1 mM $MgCl_2$, pH 7.5 and homogenized with a Dounce homogenizer using a type B pedestal. High-density sucrose (2.4 M sucrose, 10 mM Tris-HCl, 1 mM $MgCl_2$, pH = 7.5) was added to adjust the final concentration of sucrose to approximately 1.6 M. A two-layer sucrose gradient was set-up by overlaying the 1.6 M sucrose suspension with 0.25 M sucrose, 10 mM Tris-HCl, 1 mM $MgCl_2$, pH = 7.5. The sucrose gradient was centrifuged at 24,000 rpm for 70 min in a SW41 rotor. A band rich in plasma membrane and nuclei were collected. Fractionation produced ten subcellular fractions, which were subsequently analyzed by the fluorescence of Mce_6 ($\lambda_{excitation} \cong 395$ nm, $\lambda_{emission} \cong 650$ nm). Standard curves for each HPMA copolymer-Mce_6 conjugate were produced in Percoll fractions and sucrose gradients. Mce_6 concentrations were normalized to protein content per fraction (Coomassie Plus Protein Assay Reagent, Pierce).

Untreated control cells were analyzed prior to HPMA copolymer-Mce_6 conjugate exposure to characterize separation of lysosomes, plasma membrane, cytosol and nuclei for protocol described. Fractions were analyzed for hexosaminidase activity, 5′-nucleotidase activity, lactate dehydrogenase activity and ethidium bromide binding. Fractions 1 and 2 contained ~60% total lysosomal activity (hexosaminidase), whereas fraction 5 and the plasma membrane band possessed approximately 90% total plasma membrane activity (5′-nucleotidase). Seventy percent of cytosolic activity (lactate dehydrogenase) was observed in fraction 8 and the nuclear fraction contained 20 μg/mL of DNA corresponding to 40% total nucleotide content. Cell associated drug concentration (CAD) was determined by summation of lysosomal, plasma membrane, cytosolic and nuclear fractions.

Cytotoxicity Bioassay

The IC_{50} was determined utilizing a 2-(2-methoxy-4-nitrophenyl)-3-(4-nitrophenyl)-5-(2,4-disulfophenyl)-2H-tetrazolium monosodium salt (WST-8) (Dojindo) bioassay. Ten thousand cells were seeded into 96 well plates and incubated overnight in a humidified atmosphere containing 5% CO_2. Increasing concentrations of free Mce_6 or HPMA copolymer-Mce_6 conjugates were applied to cells for 4 h. Media containing free Mce_6 or drug conjugates were removed and 200 μL of fresh media was added. Cells were promptly illuminated (3 $mWcm^{-2}$) for 30 min and incubated in a humidified atmosphere containing 5% CO_2 for 72 h. The media was replaced with fresh media containing WST-8 (10 μL of WST-8 / mL of media). After a 2–3-h incubation, the absorbance was read at 450 nm with a reference wavelength at 630 nm. Untreated cells served as 100% viable cells, whereas media served as background. Linear regression was performed utilizing the linear portion of the growth inhibition curve to determine the IC_{50} dose.

Statistics

Statistical analysis was preformed utilizing Student's *t* test with a two-tailed distribution and two-sample equal variance. $P < 0.05$ was considered significant.

RESULTS

Subcellular Trafficking and Localization of HPMA Copolymer Conjugates

Confocal analysis revealed lysosomal accumulation of P-Texas Red (P1) at 37°C in A2780 cells, whereas incubation of P1 at 4°C or at 37°C in the presence of DNP significantly reduced endocytic uptake (Fig. 2). Nuclear-targeted P-NLS(FITC) (P2) also displayed lysosomal accumulation, however cytosolic, nuclear and enhanced membrane staining was observed, which was novel to P2 in comparison to P1 (Fig. 3, Panel A). Nuclear localization was confirmed by co-localization of PI (Fig. 3, Panel C) with P2 (Fig. 3, Panel D). Subcellular fractionation of A2780 cells incubated with P-GG-Mce_6 (P3) at 37°C revealed maximum uptake into lysosomes (~90%) with limited accumulation (~10%) into plasma membrane (Fig. 4). Significant inhibition of endocytosis of P3 was observed in A2780 cells incubated at either 4°C or 37°C in the presence of DNP. Similar concentrations of plasma membrane bound P3 was displayed in A2780 cells incubated with P3 at 4°C, 37°C or at 37°C in the presence of DNP. Pronounced plasma membrane binding was detected for P-GFLG-Mce_6 (P7) probably due to enhanced hydrophobic interactions, whereas nuclear-targeted HPMA copolymer

Fig. 2. Confocal microscopy of human ovarian A2780 cells incubated in the presence of P-Texas Red (100 μg/mL) in RPMI containing 10% FBS at 37°C (A), P-Texas Red (100 μg/mL) in RPMI containing 10% FBS and HEPES buffer at 4°C (B) or P-Texas Red (100 μg/mL) in RPMI containing 10% FBS in the presence of DNP (50 μg/mL) at 37°C (C). Cells seeded onto sterile glass cover slips were incubated with fluorescent conjugate for 4 h and fixed with 4% paraformaldehyde for 20 min at 37°C. Cover slips were inverted onto microscope slides utilizing antifade reagent. Slides were kept at 4°C until analysis.

conjugates (P4, P8) exhibited improved membrane binding by electrostatic interactions. A significant decrease in lysosomal accumulation was observed for P-GFLG-Mce_6 (P7) and P-NLS(FITC)-GFLG-Mce_6 (P8) at 37°C in comparison to P-GG-Mce_6 (P3) and P-NLS(FITC)-GG-Mce_6 (P4), respectively. Both P-NLS(FITC)-GG-Mce_6 (P4) and P-NLS(FITC)-GFLG-Mce_6 (P8) were identified within nuclei (~15% of CAD) with only limited detection in the cytosol (~3% of CAD). P-scNLS-GG-Mce_6 (P5) was observed in the cytosol (~10% of CAD), whereas P-NH_2-GG-Mce_6 (P6) was not. Both P5 and P6 were not detected within nuclei.

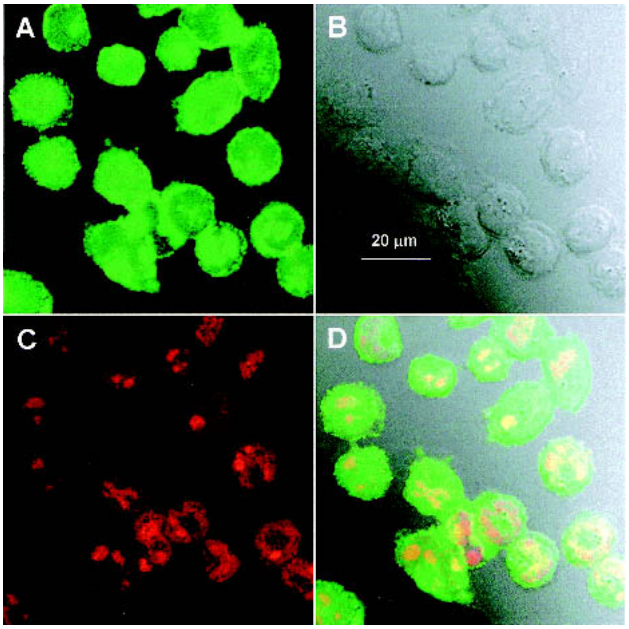

Fig. 3. Co-localization confocal microscopy of P-NLS(FITC) and PI (100 μg/mL) in human ovarian A2780 cells. Panel A: confocal microscopy of P-NLS(FITC); Panel B: transmitted light image of A2780 cells utilizing differential interference contrast optics; Panel C: nuclear localization of PI; Panel D: co-localization of P-NLS(FITC) and PI. Cells seeded onto sterile glass cover slips were incubated in the presence of P-NLS(FITC) (100 μg/mL) in RPMI containing 10% FBS at 37°C for 4 h, fixed with 4% paraformaldehyde, treated with 0.1% Triton for 4 min and incubated with DNase-free RNase (100 μg/mL) for 20 min at 37°C. Nuclei were counterstained with PI (100 μg/mL) for twenty minutes at room temperature and cover slips were inverted onto microscope slides. Slides were kept at 4°C until analysis. Untreated A2780 cells served as controls.

Cytotoxicity of HPMA Copolymer-Mce_6 Conjugates

Anti-proliferative activity of free Mce_6 or HPMA copolymer-Mce_6 conjugates to A2780 cells was assessed by growth inhibition curves. A summary of IC_{50}, IC_{90} and CAD are displayed in Table II. Inhibiting lysosomal uptake of P-GG-Mce_6 (P3) by incubation at low temperature or at 37°C in the presence of DNP reduced the IC_{50} 2-fold compared to P-GG-Mce_6 at 37°C (Fig. 5, Panel A). Additionally, the CAD for P3 at 4°C or at 37°C in the presence of DNP was approximately half compared to P3 at 37°C. P-GFLG-Mce_6 (P7) displayed a significant increase in chemotherapeutic activity compared to non-targeted P-GG-Mce_6 (P3) at 37°C. Similar CAD were observed for P3 and P7 at 37°C (Fig. 5, Panel A), whereas P7 possessed an 8-fold lower IC_{50} compared to P3 at 37°C. Both P-NLS(FITC)-GG-Mce_6 (P4) and P-NLS(FITC)-GFLG-Mce_6 (P8) possessed a 5-fold and 6-fold increase in anticancer activity compared to P-GG-Mce_6 (P3) at 37°C and P-GFLG- Mce_6 (P7), respectively. However, increased activity of P3 at 37°C could not be correlated to nuclear damage as control cationic P-scNLS(FITC)-GG-Mce_6 (P5) and P-NH_2-GG-Mce_6 (P6) conjugates exhibited similar cytotoxic activities compared to P-GG-Mce_6 (P3) at 37°C *in vitro.* In addition, cytotoxic evaluation of P-NLS(FITC)-GG-Mce_6 (P4) at 4°C generated similar growth inhibition curves as P4 at 37°C indicating chemotherapeutic activity was independent of nuclear import (Fig. 5, Panel B). P-NLS(FITC)-GFLG-Mce_6 (P8) possessed the highest chemotherapeutic activity of all HPMA copolymer-Mce_6 conjugates investigated with an approximate 10-fold increase in activity compared to P-NLS(FITC)-GG-Mce_6 (P4) at 37°C and a 5-fold increase in anticancer activity in comparison to P-scNLS(FITC)-GG-Mce_6 (P5) and P-NH_2-Mce_6 (P6) normalizing for CAD (Fig. 3, Panel B). Analysis of the anti-proliferative activity of P-NLS(FITC)-GFLG-Mce_6 (P8) at 4°C revealed a slightly altered growth inhibition curve compared to P8 at 37°C (Fig. 3, Panel B).

Photodamage Induced in A2780 Cells

The induction of photodamage induced by HPMA copolymer-Mce_6 conjugates was investigated by morphologic analysis utilizing confocal microscopy. Photodamage induced by P-GG-Mce_6 (P3) at 4°C and at 37°C in the presence of DNP was not investigated further as only moderate enhancements in cytotoxicity was observed compared to P3 at 37°C.

Apoptosis as observed by uniform condensed nuclear chromatin was visible in A2780 cells exposed to free Mce_6 or HPMA copolymer-Mce_6 conjugates immediately following illumination (Fig. 6). Condensed nuclei were detected 2 h and 4 h postactivation with the exception of P-GG-Mce_6 (P3) at 37°C, where nuclear condensation was not observed until 4 h post illumination (Fig. 6, Panels E-F). Irregular clumping of chromatin symbolic of necrotic death was visible in A2780 cells treated with P-NLS(FITC)-GFLG-Mce_6 (P8) directly following induction of photodamage (Fig. 6, Panel M). Co-localization of MitoFluor™ Far Red and LysoTracker®

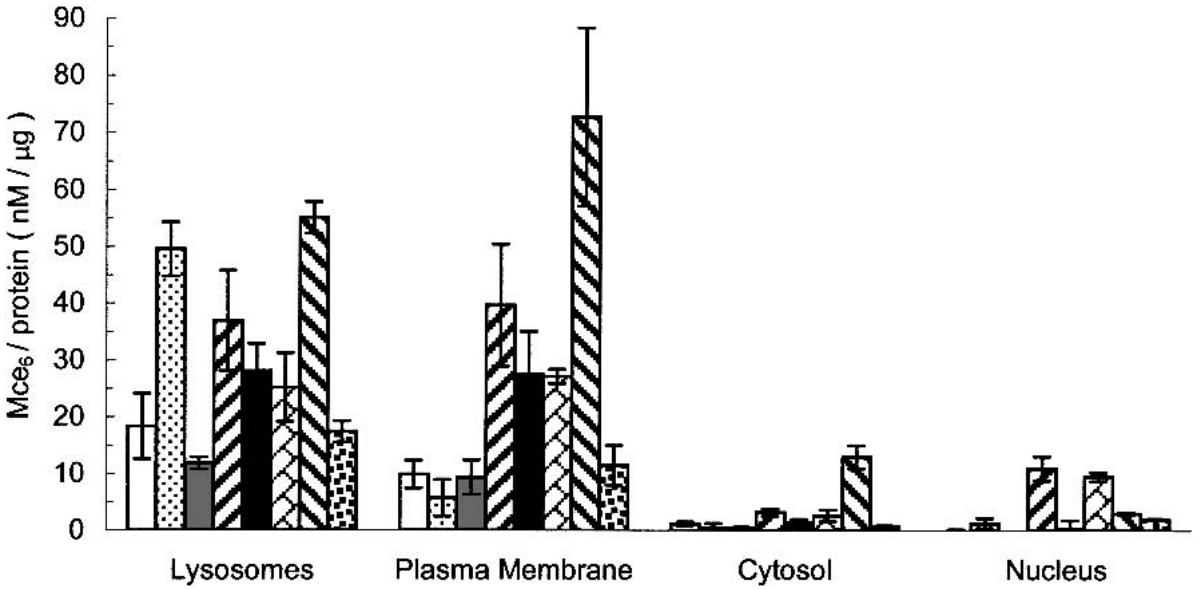

Fig. 4. Subcellular distribution of HPMA copolymer-Mce$_6$ conjugates (100 μM) in human ovarian A2780 cells. Subcellular localization of P-GG-Mce$_6$ at 4°C (□), P-GG-Mce$_6$ at 37°C ,(⊡), P-GG-Mce$_6$ in the presence of DNP (50 μg/mL) at 37°C (▭), P-NLS(FITC)-GG-Mce$_6$ at 37°C (▨), P-GFLG-Mce$_6$ at 37°C (■), P-NLS(FITC)-GFLG-Mce$_6$ at 37°C (▩), P-scNLS(FITC)-GG-Mce$_6$ at 37°C (▧) or P-NH$_2$-GG-Mce$_6$ at 37°C (▩) in A2780 cells. Cells were incubated with conjugates for 4 h, homogenized and centrifuged. The supernatant was applied to 23% Percoll, whereas the pellet was purified utilizing a sucrose gradient. Samples were analyzed by the fluorescence of copolymer bound Mce$_6$ ($\lambda_{excitation} \cong 395$ nm, $\lambda_{emission} \cong 650$ nm). Concentrations of HPMA copolymer-Mce$_6$ conjugates were determined by generating standard curves of HPMA copolymer-Mce$_6$ conjugates in Percoll fractions or sucrose fractions containing untreated cells. Fractionation was performed in duplicate except for P-GG-Mce$_6$ at 37°C and P-GFLG-Mce$_6$ at 37°C, which was performed in quadruplicate. Data sets represent mean ± S.D.

Green DND-26 was detected in A2780 cells treated with free Mce$_6$ and P-GG-Mce$_6$ (P3) at 37°C 2 h post illumination indicating lysosomal and mitochondrial integrity was compromised in these cells (data not shown).

DISCUSSION

PDT is an emergent method of anticancer treatment. To optimize the therapeutic effect of photosensitizers many parameters have been investigated. Second-generation photosensitizers have been identified which absorb more strongly at longer wavelengths affording deeper tissue penetration and are cleared from the body more rapidly reducing skin photosensitivity following treatment. Enhanced tumor uptake has been achieved by way of conjugation of sensitizers to macromolecular delivery systems, which has been further increased by the addition of targeting moieties. Elucidation of PDT sensitive subcellular targets is still being explored. This task becomes more difficult as correlations vary for cell type, cell line, photosensitizer, dose, and light energy used.

Free Mce$_6$ was attached to HPMA copolymers utilizing a non-degradable dipeptide spacer (GG) or a degradable tetrapeptide linker (GFLG) to evaluate chemotherapeutic activity between copolymer-bound Mce$_6$ and enzymatically released Mce$_6$. It has previously been reported the quantum yield of singlet oxygen generation was significantly higher for free Mce$_6$ in comparison to HPMA copolymer-Mce$_6$ conjugates (12). HPMA copolymers containing hydrophobic moieties were shown to form micelle like structures in aqueous buffers (17). Aggregation of HPMA copolymer-Mce$_6$ conjugates influenced by Mce$_6$ loading and side-chain hydrophobicity may interfere with the ability of molecular oxygen to access Mce$_6$ within the hydrophobic core or singlet oxygen to diffuse out of the copolymer structure. Cleavage of P-GFLG-Mce$_6$ with cathepsin B increased the quantum yield of singlet oxygen to comparable levels as free Mce$_6$ (18). Cytotoxic evaluation of P-GFLG-Mce$_6$ (P7) corroborate the enzymatic release of free Mce$_6$ *in vitro* as an 8-fold decrease in IC_{50} was observed compared to P-GG-Mce$_6$ (P3) at 37°C, although similar CADs were observed for both conjugates.

Inhibiting lysosomal uptake of P-GG-Mce$_6$ (P3) in A2780 cells utilizing incubation at low temperature (4°C) or incubation at 37°C in the presence of a metabolic inhibitor (DNP) reduced the IC_{50} 2-fold compared to incubation of A2780 cells with P3 at 37°C. Subcellular distribution of P3 at 4°C, 37°C and at 37°C in the presence of DNP varied only in lysosomal accumulation indicating an insensitivity of lysosomes to photodamage. Discrepancies have been reported for lysosomal damage. In murine leukemia cells, a limited apoptotic response was displayed for lysyl chlorin e$_6$, lutetium texaphyrin and *N*-aspartyl chlorin e$_6$; although, an immediate loss of lysosomal integrity was observed upon illumination (19). Additionally, a lack of lysosomal photodamage was displayed in the same cell line treated with an acetomethyl ester of chlorin e$_6$ (20). In contrast, photoactivation of lutetium texaphyrin led to lysosomal breakup, extensive cytoplasmic blebbing and subsequent death in a murine mammary sarcoma (21). Treatment of human colon adenocarcinoma cells with *meta*-tetra(hydroxyphenyl)chlorin led to a rapid apoptotic response on photodamage elicited within lysosomes (22). These inconsistencies may be explained by inactivation of lysosomal hydrolases. The inactivation of lysosomal en-

Table II. Cytotoxicity of HPMA Copolymer-Mce_6 Conjugates to Human Ovarian A2780 Cells and Cell Associated Drug Concentrations (CAD)

	Conjugates	IC_{50} ± SD (μM)	IC_{90} ± SD (μM)	CAD ± SD (nM)
	Free Mce_6	2.0 ± 0.4[a]	3.1 ± 0.5[a]	nd
P3	P(GG)-Mce_6 4°C	34.8 ± 7.1[b]	71.2 ± 13.1[b]	29.2 ± 4.0[c]
P3	P(GG)-Mce_6 37°C	76.3 ± 6.4[d]	121.6 ± 22.3[d]	56.4 ± 1.3[c]
P3	P(GG)-Mce_6 37°C + DNP (50 μg/mL)	28.6 ± 1.9[b]	39.3 ± 1.4[b]	20.6 ± 1.8[c]
P4	P-NLS(FITC)-GG-Mce_6 4°C	12.6 ± 3.7[d]	22.3 ± 5.9[d]	nd[c]
P4	P-NLS(FITC)-GG-Mce_6 37°C	9.6 ± 3.7[a]	16.4 ± 6.1[a]	90.6 ± 22.3
P5	P-scNLS(FITC)-GG-Mce_6 37°C	3.3 ± 0.4[c]	6.1 ± 0.9[c]	143.6 ± 14.6[c]
P6	P-NH_2-GG-Mce_6 37°C	13.7 ± 0.1[c]	21.5 ± 0.3[c]	31.5 ± 5.7[c]
P7	P(GFLG)-Mce_6 37°C	9.6 ± 0.8[b]	15.9 ± 1.5[b]	57.9 ± 3.5[c]
P8	P-NLS(FITC)-GFLG-Mce_6 4°C	1.7 ± 0.2[c]	2.9 ± 0.6[c]	nd
P8	P-NLS(FITC)-GFLG-Mce_6 37°C	1.4 ± 0.0[c]	2.6 ± 0.0[c]	64.4 ± 7.6[c]

Note: For cytotoxicity, cells were incubated with increasing concentrations of free Mce_6 or HPMA copolymer-Mce_6 conjugates for 4 h, media containing drug or drug conjugates was replaced with fresh media, cells were irradiated 30 minutes (3 mW/cm^2) and incubated 72 h in a humidified atmosphere containing 5% CO_2. Viability was assessed utilizing a WST-8 bioassay. Linear regression was performed to determine the IC_{50} and IC_{90} doses. For CAD, cells were exposed to HPMA copolymer-Mce_6 conjugates (100 μM) for 4 h and fractionated as described in Materials and Methods. The summation of lysosomal, plasma membrane, cytosolic, and nuclear fractions yielded the CAD. Values are mean ± S.D. (N = separate number of experiments).

[a] N = 5.
[b] N = 4.
[c] N = 2.
[d] N = 3.

zymes was reported for aluminum phthalocyanines, that varied on the degree of sulfonation. Tetrasulfonated tetraphenyl porphines completely abolished the activity of cathepsins in human cervix carcinoma cells, whereas 30–50% inactivation was observed for mono- and disulfonated tetraphenyl porphines (23). Additionally, cathepsins were inactivated in Chinese hamster lung fibroblasts on light exposure when aluminum phthalocyanines were present (24). Cysteine cathepsins are a major contributor to cytotoxicity on lysosomal disruption in human fibroblasts (25). Inactivation of these hydrolases may protect cells from the cytotoxic action upon lysosomal disruption. Variations in sensitivity of lysosomes to PDT may also vary for the structural properties of photosensitizers. Hydrophobic sensitizers may elicit photodamage at the lysosomal membrane. In comparison, hydrophilic sensitizers may damage components within the endocytic vesicles. Cytosol inhibition of cathepsin activity was demonstrated in human cervix carcinoma cells (23). Cathepsin activity and the concentration of cathepsin inhibitors present within the cytosol has also been shown to vary for cells from different neoplastic diseases providing an alternate explanation to variations in the sensitivity of lysosomes to PDT (26).

NLS was covalently coupled to HPMA copolymer-Mce_6 conjugates containing Mce_6 bound by non-degradable or degradable spacers. Fractionation studies described a slight reduction in lysosomal accumulation of P-NLS(FITC)-GFLG-Mce_6 (P8) in comparison to P-NLS(FITC)-GG-Mce_6 (P4) indicating free Mce_6 was liberated from lysosomally accumulated P-NLS(FITC)-GFLG-Mce_6 (P8). Comparable nuclear delivery (~15% of CAD) was observed for P-NLS(FITC)-GG-Mce_6 (P4) and P-NLS(FITC)-GFLG-Mce_6 (P8) describing similar efficiencies of P4 and P8 to traverse biologic membranes resulting in cytoplasmic and ultimately nuclear delivery. Additionally, confocal microscopy studies described cytoplasmic delivery of P-NLS(FITC) (P2) at 4°C indicating cytoplasmic delivery of nuclear-targeted conjugates was independent of lysosomal uptake with direct interaction with plasma membrane. P4 displayed enhanced membrane accumulation (~35% of CAD) and a significant decrease in lysosomal compartmentalization (~40% of CAD) compared to the non-targeted parent conjugate (P3). Equivalent levels of membrane accumulation were observed for P8 and the non-targeted parent conjugate (P7). The only distinction was

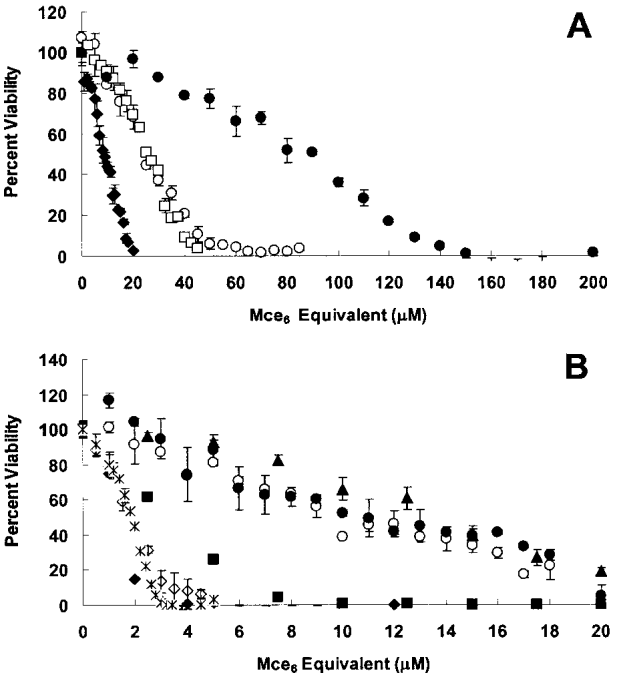

Fig. 5. Growth inhibition curves of HPMA copolymer-Mce_6 conjugates to human ovarian A2780 cells. In panel A, the cytotoxicity of non-targeted HPMA copolymer-Mce_6 conjugates (P-GG-Mce_6 at 4°C (○), P-GG-Mce_6 at 37°C (●), P-GG-Mce_6 in the presence of DNP (50 μg/mL) at 37°C (□) and P-GFLG-Mce_6 at 37°C (♦)) are displayed. In panel B, the cytotoxicity of nuclear-targeted and non-targeted cationic HPMA copolymer-Mce_6 conjugates (P-NLS(FITC)-GG-Mce_6 at 4°C (○), P-NLS(FITC)-GG-Mce_6 at 37°C (●), P-scNLS(FITC)-GG-Mce_6 at 37°C (■), P-NH_2-GG-Mce_6 at 37°C (▲), P-NLS(FITC)-GFLG-Mce_6 at 4°C (◇), and P-NLS(FITC)-GFLG-Mce_6 at 37°C (♦)) are shown. HPMA copolymer-Mce_6 conjugates were exposed to cells for 4 h, illuminated for 30 min (3 mW/cm^2) and incubated in a humidified atmosphere containing 5% CO_2 for 72 h. Viability was assessed utilizing a WST-8 bioassay. Each data point represents mean ± S.D. in duplicate.

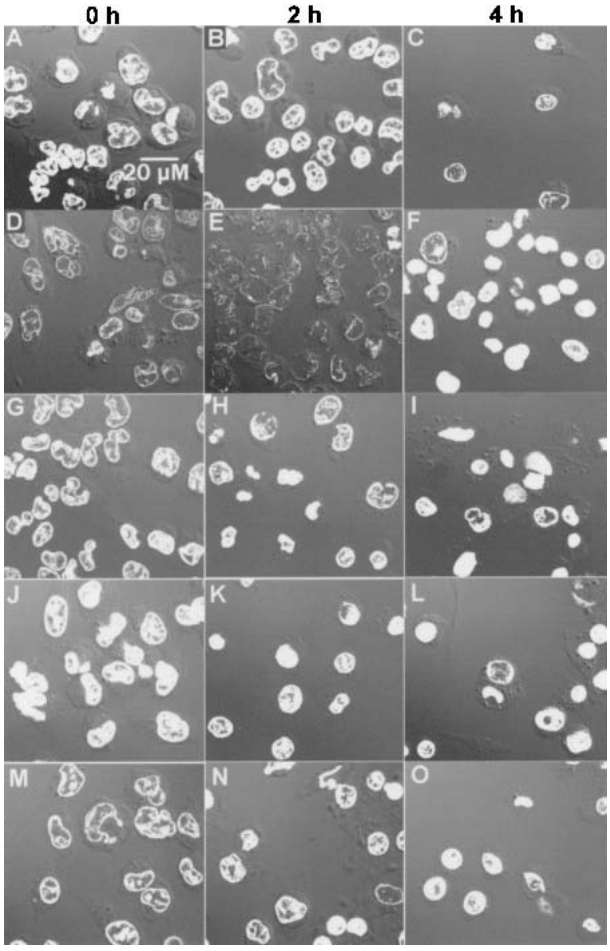

Fig. 6. Alterations in nuclear morphology in A2780 cells upon photoactivation of free Mce$_6$ (A-C), P-GG-Mce$_6$ (D-F), P-NLS(FITC)-GG-Mce$_6$ (G-I), P-GFLG-Mce$_6$ (J-L) or P-NLS(FITC)-GFLG-Mce$_6$ (M-O). Cells were incubated with drug or drug conjugate for 4 h and illuminated for 30 min (3 mW/cm^2). Thirty minutes prior to fixation with 4% paraformaldehyde, media was supplemented with Hoechst 33342 (1 μM). Slides were kept at 4°C until analysis.

the nuclear delivery observed for P8. Other macromolecular PDT delivery systems have been described utilizing NLS from simian virus large tumor antigen. Conjugates have been constructed incorporating NLS-β-galactosidase fusion protein as carriers to which chlorin e$_6$ and insulin were successively linked (27). Incorporation of flanking regions of the minimal NLS (amino acids 126–132) has been shown to alter nuclear import. Specifically, Ser$_{112}$ increased the rate of nuclear import 50-fold, whereas phosphorylation of Thr$_{124}$ decreased maximal nuclear delivery (28). For the NLS-chlorin e$_6$-insulin constructs, amino acids 111–135 from the NLS were included with the alteration of T124A to eliminate the inhibitory phosphorylation site. Nuclear delivery as observed by confocal laser scanning microscopy described a nuclear/cytoplasmic localization ratio (N/C) of 0.88 (10). Chlorin e$_6$ peptides were prepared by coupling chlorin e$_6$ to NLS(APPKKKRKVEDP$_{135}$)-cytoplasmic translocation domain(pentalysine) peptide during solid-phase synthesis (11). A branched construct termed loligomers was also synthesized incorporating eight identical chlorin e$_6$-peptide arms. Both delivery systems harbored the threonine to alanine substitution. Quantification of gold particles in electron micrographs utilizing biotinylated ce$_6$-peptides or loligomers displayed an approximate N/C ratio of approximately 0.4 and 1.4, respectively. Studies did not elaborate on the distribution of the NLS-chlorin e$_6$-insulin, chlorin e$_6$-peptide or loligomers in other subcellular organelles such as plasma membrane or endocytic compartments. For P-NLS(FITC)-GG-Mce$_6$ (P4) the N/C ratio was approximately 3.8 and the N/C ratio of P-NLS(FITC)-GFLG-Mce$_6$ (P8) was 3.6. These ratios are misleading, because the majority of P4 and P8 were found within plasma membrane and lysosomes. A nucleus/CAD ratio for P4 and P8 was approximately 0.15. Conjugation of cationic NLS or scNLS to HPMA copolymer-Mce$_6$ conjugates significantly enhanced non-specific interactions with the plasma membrane because of favorable electrostatic interactions. Similar findings were described for polylysine chlorin e$_6$ conjugates (29). For P-GFLG-Mce$_6$ (P7), plasma membrane binding was improved compared to P-GG-Mce$_6$ due to increased hydrophobic interactions compared to P3. Significant enhancement in membrane binding for P-NLS(FITC)-GFLG-Mce$_6$ (P8) in comparison to P7 was not displayed. To improve nuclear delivery of HPMA copolymer-Mce$_6$ the incorporation of flanking sequences of the NLS could be used. Additionally, higher contents of NLS can be bound per copolymer chain. However, problems associated with increasing the cationic nature per copolymer such as membrane binding and toxicity must be addressed.

Improved chemotherapeutic activity was observed for P4 and P8, but further analysis revealed control cationic HPMA copolymer-Mce$_6$ conjugates containing a scrambled NLS sequence (P5) or primary amino groups (P6) also possessed enhanced anticancer activity compared to P-GG-Mce$_6$ (P3) at 37°C. Normalizing the IC$_{50}$ to CAD is essential to determine the efficacy of HPMA copolymer-Mce$_6$ conjugates. P4 possessed similar chemotherapeutic action as P-scNLS(FITC)-GG-Mce$_6$ (P5) and P-NH$_2$-GG-Mce$_6$ (P6). Additionally, cytotoxic evaluation of P4 at 4°C and 37°C was indistinguishable. The lower IC$_{50}$ observed for P4 was caused by enhanced cellular uptake and was not dependent on photodamage elicited within the nucleus. In contrast, enhanced anticancer activity of P-NLS(FITC)-GFLG-Mce$_6$ (P8) could not solely be correlated to increased cellular uptake, because P8 was 5 times more efficient than control cationic conjugates (P5, P6). In addition, cytotoxic evaluation of P8 at 4°C described a slight increase in IC$_{50}$ compared to incubation at 37°C. Differences in chemotherapeutic activity between P4 and P8 may be caused by the generation of enzymatically released Mce$_6$ from lysosomally accumulated P8 as released Mce$_6$ has a higher quantum yield in singlet oxygen compared to copolymer-bound Mce$_6$ (P4). Irregular chromatin condensation indicative of necrosis was more evident in A2780 cells treated with P8 in comparison to other HPMA copolymer-Mce$_6$ conjugates (P3, P4, and P7). Photoinduced membrane rupture was hypothesized to undergo two parallel processes: first, lipid peroxidation by way of singlet oxygen and second, aggregation of damaged lipids to form a separate phase from the undamaged lipid membranes. In conjunction, these processes led to membrane lysis. It is unclear why P-NLS(FITC)-GFLG-Mce$_6$ (P8) exhibited a higher necrotic response as similar amounts of P4, P7, and P8 were detected within plasma membrane. Possible explanations include variances in singlet oxygen generation for different HPMA copolymer-

Mce_6 conjugates. Although HPMA copolymers form micelle-like structures, the introduction of cationic charge most likely altered its secondary structure and photoproperties. Enhanced activity has been reported for NLS-chlorin e_6-insulin conjugates with a 2000-fold decrease in IC_{50} compared to chlorin e_6 in insulin-receptor bearing human hepatoma cells (10). However, only a 4-fold decrease was observed for NLS-chlorin e_6-insulin constructs compared to chlorin e_6-insulin conjugates containing wild-type β-galactosidase containing no NLS insert. Treatment of Chinese hamster ovarian carcinoma or in murine fibrosarcoma RIF-1 cells with chlorin e_6-peptide or loligomers improved the photodynamic efficiency 1 or more magnitudes compared to chlorin e_6 with loligomers possessing the highest anticancer activity (11). These results illustrate the importance of differentiating enhanced chemotherapeutic efficacy because of enhanced cellular uptake vs. nuclear damage. The inadvertent addition of cationic charge by incorporation of NLS may alter the growth inhibition curve due to improved membrane binding. Studies are required to correlate preferential subcellular damage with mechanisms of cytotoxicity and cellular responses.

In summary, many factors must be considered when selecting an optimal HPMA copolymer-Mce_6 delivery system. A compromise must be made between photodynamic activity and desirable mechanism of cell death. Lysosomes appeared less sensitive to photodamage compared to plasma membrane, but this effect was not dramatic. Targeting the plasma membrane may be advantageous, as cationic HPMA copolymer-Mce_6 conjugates possessed increased chemotherapeutic activity; however, membrane lysis representative of necrosis has been reported on membrane damage (31). Side effects associated with necrotic vs. apoptotic death on PDT needs to be explored. Although nuclear-directed HPMA copolymer-Mce_6 conjugates (P4, P8) possessed desirable chemotherapeutic activity, control cationic HPMA copolymer-Mce_6 conjugates (P5, P6) also exhibited similar enhancements in chemotherapeutic effect due to favorable electrostatic interactions with the plasma membrane. Enhancement in chemotherapeutic activity caused by membrane accumulation vs. nuclear damage must be differentiated as non-specific electrostatic interactions of cationic nuclear-targeted PDT systems with the plasma membrane may overwhelm the PDT system. Although the plasma membrane may be desirable PDT target, studies have described a delay or prevention of apoptosis on membrane damage (30). Further studies are warranted to validate the use of cationic nuclear localization sequences to enhance chemotherapeutic activity by generating nuclear damage.

ACKNOWLEDGMENTS

This research was supported by NIH grant CA 51578 from the National Cancer Institute and an Advanced Predoctoral Fellowship in Pharmaceutics from PhRMA Foundation. The authors thank Jerry Kaplan and Diane McVey Ward for helpful discussions.

REFERENCES

1. J. Moan and K. Berg. The photodegradation of porphyrins in cells can be used to estimate the lifetime of singlet oxygen. *Photochem. Photobiol.* **53**:549–553 (1991).
2. Q. Peng, J. Moan, and J. M. Nesland. Correlation of subcellular and intratumoral photosensitizer localization with ultrastructural features after photodynamic therapy. *Ultrastruct. Pathol.* **20**:109–129 (1996).
3. Q. Peng, J. Moan, L. W. Ma, and J. M. Nesland. Uptake, localization, and photodynamic effect of meso-tetra(hydroxyphenyl-)porphine and its corresponding chlorin in normal and tumor tissues of mice bearing mammary carcinoma. *Cancer Res.* **55**: 2620–2626 (1995).
4. Y. Matsumura and H. Maeda. A new concept for macromolecular therapeutics in cancer chemotherapy: mechanism of tumoritropic accumulation of proteins and the antitumor agent SMANCS. *Cancer Res.* **46**:6387–6392 (1986).
5. H. F. Dvořák, J. A. Nagy, J. T. Dvořák, and A. M. Dvořák. Identification and characterization of the blood vessels of solid tumors that are leaky to circulating macromolecules. *Am. J. Pathol.* **133**:95–109 (1988).
6. J. W. Baish, P. A. Netti, and R. K. Jain. Transmural coupling of fluid flow in microcirculatory network and interstitium in tumors. *Microvasc. Res.* **53**:128–141 (1997).
7. J. G. Shiah, Y. Sun, C. M. Peterson, and J. Kopeček. Biodistribution of free and N-(2-hydroxypropyl)methacrylamide copolymer- bound mesochlorin $e_{(6)}$ and adriamycin in nude mice bearing human ovarian carcinoma OVCAR-3 xenografts. *J. Control. Release* **61**:145–157 (1999).
8. J. Kopeček, P. Kopecková, T. Minko, and Z. Lu. HPMA copolymer-anticancer drug conjugates: design, activity, and mechanism of action. *Eur. J. Pharm. Biopharm.* **50**:61–81 (2000).
9. Z. R. Lu, P. Kopečková, and J. Kopeček. Polymerizable Fab′ antibody fragments for targeting of anticancer drugs. *Nat. Biotechnol.* **17**:1101–1104 (1999).
10. T. V. Akhlynina, D. A. Jans, A. A. Rosenkranz, N. V. Statsyuk, I. Y. Balashova, G. Toth, I. Pavo, A. B. Rubin, and A. S. Sobolev. Nuclear targeting of chlorin e_6 enhances its photosensitizing activity. *J. Biol. Chem.* **272**:20328–20331 (1997).
11. S. K. Bisland, D. Singh, and J. Gariépy. Potentiation of chlorin e_6 photodynamic activity *in vitro* with peptide-based intracellular vehicles. *Bioconjug. Chem.* **10**:982–992 (1999).
12. N. L. Krinick, Y. Sun, D. Joyner, J. D. Spikes, R. C. Straight, and J. Kopeček. A polymeric drug delivery system for the simultaneous delivery of drugs activatable by enzymes and/or light. *J. Biomater. Sci. Polym. Ed.* **5**:303–324 (1994).
13. R. Duncan and J. B. Lloyd. Pinocytosis in the rat visceral yolk sac. Effects of temperature, metabolic inhibitors and some other modifiers. *Biochim. Biophys. Acta* **544**:647–655 (1978).
14. J. Kopeček and H. Bažilová. Poly[N-(2-hydroxypropyl)methacrylamide]. 1. Radical polymerization and copolymerization. *Europ. Polym. J.* **9**:7–14 (1973).
15. P. Rejmanová, J. Labský, and J. Kopeček. Aminolyses of monomeric and polymeric p-nitrophenyl esters of methacryloylated amino acids. *Makromol. Chem.* **178**:2159–2168 (1977).
16. H. R. Yen, J. Kopeček, and J. D. Andrade. Optically controlled ligand delivery. 1. Synthesis of water-soluble copolymers containing photocleavable bonds. *Makromol. Chem.* **190**:69–82 (1989).
17. K. Ulbrich, C. Koňák, Z. Tuzar, and J. Kopeček. Solution properties of drug carriers based on poly[N-(2-hydroxypropyl)methacrylamide] containing biodegradable bonds. *Makromol. Chem.* **188**:1261–1272 (1987).
18. J. D. Spikes, N. L. Krinick. and J. Kopeček. Photoproperties of a mesochlorin e_6 - N-(2-hydroxypropyl)methacrylamide copolymer conjugate. *J. Photochem. Photobiol. A: Chem.* **70**:163–170 (1993).
19. D. Kessel, Y. Luo, P. Mathieu, and J. J. Reiners Jr. Determinants of the apoptotic response to lysosomal photodamage. *Photochem. Photobiol.* **71**:196–200 (2000).
20. D. Kessel and R. D. Poretz. Sites of photodamage induced by photodynamic therapy with a chlorin e_6 triacetoxymethyl ester (CAME). *Photochem. Photobiol.* **71**:94–96 (2000).
21. K. W. Woodburn, Q. Fan, D. R. Miles, D. Kessel, Y. Luo, and S. W. Young. Localization and efficacy analysis of the phototherapeutic lutetium texaphyrin (PCI-0123) in the murine EMT6 sarcoma model. *Photochem. Photobiol.* **65**:410–415 (1997).
22. W. N. Leung, X. Sun, N. K. Mak, and C. M. Yow. Photodynamic effects of mTHPC on human colon adenocarcinoma cells: photocytotoxicity, subcellular localization and apoptosis. *Photochem. Photobiol.* **75**:406–411 (2002).

23. K. Berg. and J. Moan. Lysosomes as photochemical targets. *Int. J. Cancer* **59**:814–822 (1994).
24. J. Moan, K. Berg, H. Anholt, and K. Madslien. Sulfonated aluminium phthalocyanines as sensitizers for photochemotherapy. Effects of small light doses on localization, dye fluorescence and photosensitivity in V79 cells. *Int. J. Cancer* **58**:865–870 (1994).
25. P. D. Wilson, R. A. Firestone, and J. Lenard. The role of lysosomal enzymes in killing of mammalian cells by the lysosomotropic detergent N-dodecylimidazole. *J. Cell Biol.* **104**:1223–1229 (1987).
26. T. T. Lah, M. Kokalj–Kunovar, B. Strukelj, J. Pungercar, D. Barlic–Maganja, M. Drobnic–Kosorok, L. Kastelic, J. Babnik, R. Golouh, and V. Turk. Stefins and lysosomal cathepsins B, L and D in human breast carcinoma. *Int. J. Cancer* **50**:36–44 (1992).
27. A. A. Rosenkranz, D. A. Jans, and A. S. Sobolev. Targeted intracellular delivery of photosensitizers to enhance photodynamic efficiency. *Immunol. Cell Biol.* **78**:452–464 (2000).
28. D. A. Jans and S. Hubner. Regulation of protein transport to the nucleus: central role of phosphorylation. *Physiol. Rev.* **76**:651–685 (1996).
29. N. S. Soukos, M. R. Hamblin, and T. Hasan. The effect of charge on cellular uptake and phototoxicity of polylysine chlorin(e_6) conjugates. *Photochem. Photobiol.* **65**:723–729 (1997).
30. D. Kessel, Y. Luo, Y. Deng, and C. K. Chang. The role of subcellular localization in initiation of apoptosis by photodynamic therapy. *Photochem. Photobiol.* **65**:422–426 (1997).
31. W. P. Thorpe, M. Toner, R. M. Ezzell, R. G. Tompkins, and M. L. Yarmush. Dynamics of photoinduced cell plasma membrane injury. *Biophys. J.* **68**:2198–2206 (1995).